Chapter 3

Ion-Beam Modified Terahertz GaAs Photoconductive Antenna

Caiming Sun and Aidong Zhang

Additional information is available at the end of the chapter

http://dx.doi.org/10.5772/intechopen.79693

Abstract

Ion-implanted photoconductive GaAs terahertz (THz) antennas were demonstrated to deliver both high-efficiency and high-power THz emitters, which are attributed to excellent carrier acceleration and fast carrier trapping for THz generations by analyzing ultrafast carrier dynamics at subpicosecond scale. The implantation distance at over 2.5 μm is deep enough to make defects (Ga vacancies, As_{Ga}^{+}…, etc.) quite few; hence, a few with good mobility similar to bare GaAs ensures excellent carrier acceleration in shallow distance <1.0 μm as photo carriers are generated by the pump laser. The implantation dosage is carefully optimized to make carrier trapping very fast, and screen effects by photo-generated carriers are significantly suppressed, which increases the THz radiation power of SI-GaAs antennas by two orders of magnitude. Under the same photoexcitation conditions (pump laser power, bias voltage), photocurrents from GaAs antennas with optimum conditions 300 keV, 5×10^{14} cm^{-2} for H implantation are decreased by two orders of magnitude; meanwhile, the THz radiation is enhanced by over four times, which means that the electrical-to-THz power conversion efficiency is improved by a factor of over 1600.

Keywords: terahertz antenna, ion-beam technology, electrical-to-THz power conversion efficiency, photoconductive antenna, semi-insulating GaAs, ion-implantation

1. Introduction

The development of a terahertz (THz) source has obtained much interest over the last three decades due to their widespread scientific and military applications [1–3]. Photoconductive antennas (PCAs) illuminated by a femtosecond (fs) laser have been becoming the dominant methods for intense THz radiations [3] since the pioneering demonstration of picosecond

photoconducting Hertzian dipoles in 1984 [4]. Historically, commercial semi-insulating (SI)-GaAs grown by liquid-encapsulated Czochralski has been the cost-effective choice as the substrate for PCAs, due to its high resistivity (>10^7 Ω cm) and high electron mobility (μ > 7000 cm^2/Vs) [5]. Afterward, about 1 μm-thick film of low-temperature (LT) grown GaAs (LT-GaAs) by molecular beam epitaxy (MBE) on the surface of SI-GaAs substrate is extensively used to reduce carrier lifetime to below 1 ps with high resistivity (10^7 Ω cm) and relatively reasonable mobility μ (100–300 cm^2/Vs) [6, 7], in order to efficiently generate broadband THz radiations of over 1 THz and reduce the carrier lifetime of PCAs on SI-GaAs (τ > 100 ps). An alternative approach for short lifetime is to create point defects in SI-GaAs by ion-implantation technique. Arsenic, oxygen, nitrogen, carbon, hydrogen (proton), etc., have been implanted into SI-GaAs and the obtained GaAs PCAs are similar to those on LT-GaAs [8–11]. However, the process conditions for either LT-GaAs or ion-implanted GaAs are not easy to reproduce in mass production, because of the difficult control of low-temperature process for MBE [12, 13], extremely high implantation energies (∼MeV) for heavy ions [11] and the challenging control for post annealing at relatively low temperatures [8, 14].

Fundamentally, the THz radiation power and optical-to-THz conversion efficiency for GaAs PCAs illuminated by femtosecond laser pulses are proportional to the photoconductive material factor $\mu\tau^2$ of PCAs [15]. The reduced electron mobility and carrier lifetime as mentioned earlier will seriously affect the THz power and conversion efficiency [3, 16, 17]. The radiation mechanism is attributed to a time-varying current, a result of photo carriers accelerating across photoconductive gap in the presence of applied electrical field [18]. The emitted THz pulse energy is derived from that stored in the static bias field [19]. Grischkowsky has reported that an extremely strong field exists near the anode of electrically biased PCAs [20], and Salem also demonstrated that THz amplitude can be multiplied by many times when the focused laser beam moved to the anode of an ion-implanted GaAs antenna at the same bias voltage [9]. Recently, plasmonic contact electrodes were used to enhance light absorption within distances of ∼100 nm from the anode and 7.5% optical-to-THz conversion efficiency was recorded at very low pump densities of <10 μJ/cm^2 [21]. However, a tightly focused laser beam will cause a high screening effect [22] and the THz power from PCA becomes lower and lower as optical pump saturates [23, 24], which principally sets an upper limit for the conversion efficiency of THz radiations. Thus, it is critical to find out a strategy of creating sufficient defects to reduce the carrier lifetime without affecting mobility detrimentally. High-energy and low-dosage ion-implantation has been verified to be an efficient method of creating proper profiles of defects, in order to obtain both excellent carrier acceleration at the shallow region and fast carrier trapping at the deep layer for THz generations [11, 25]. Also, hydrogen implantation is extensively used to separate high-power active devices (IGBT, laser diodes, LED, etc.) from their mother substrate and get superior performance of high frequency and high efficiency.

2. Experimental results and discussions

In this work, the photoconductive antenna substrate was a commercial high-resistivity (5×10^7 Ω cm), liquid-encapsulated Czochralski-grown, (100)-oriented, semi-insulating (SI)-GaAs

wafer. A 10/200 nm-thick Ti/Au metal layer stack was deposited on GaAs substrate by e-beam evaporation, functioning as metal electrodes for PCAs. The PCA has a bow-tie antenna structure with a photoconductive gap of 0.4 mm, 90° bow angle, and antenna length of 2 mm, as shown in **Figure 1(a)**. Afterward, ion beam for hydrogen, helium, or oxygen was implanted into such SI GaAs PCAs with penetration depth of 2.5 μm and the acceleration energies are 300 keV, 800 keV, 3 MeV for H, He, O respectively. Implantation energies were selected so that the peak of ion concentration profile is situated deeper than the thickness of THz-relevant layer within SI-GaAs antenna, which is ~2 μm. The implantation dosage varied from 1×10^{12} to 1×10^{15} cm^{-2}, where lower dose and higher energies were used for heavier ions whereas higher dose and lower energies were suitable for lighter ions. The process details for all samples with different implantation conditions are shown in **Table 1**.

As discussed in our previous work [25], 300 keV H implantation was an easily reproducible condition for fabricating SI-GaAs PCAs with ion penetration depth of 2.5 μm, effectively defining the active region for THz generations. The implantation dosage of H ions varied from 1×10^{14} to 1×10^{15} cm^{-2}, to find out optimum conditions for ion-implanted GaAs PCAs. Density profiles of the generated defects and the implanted ions were optimized by the stopping and range of ions in matter (SRIM) program [26], and the peak distribution situates as deep as 2.5 μm distance from PCA surface. The defects concentration in shallow regions (<1 μm deep) are over three orders of magnitude lower than the peak concentration at 2.5 μm distance, where most photo carriers are generated under femtosecond laser excitation and accelerated at local electrical fields for THz generations. As carriers transit into defects-rich regions underneath the acceleration layer, they will be efficiently trapped and the carrier

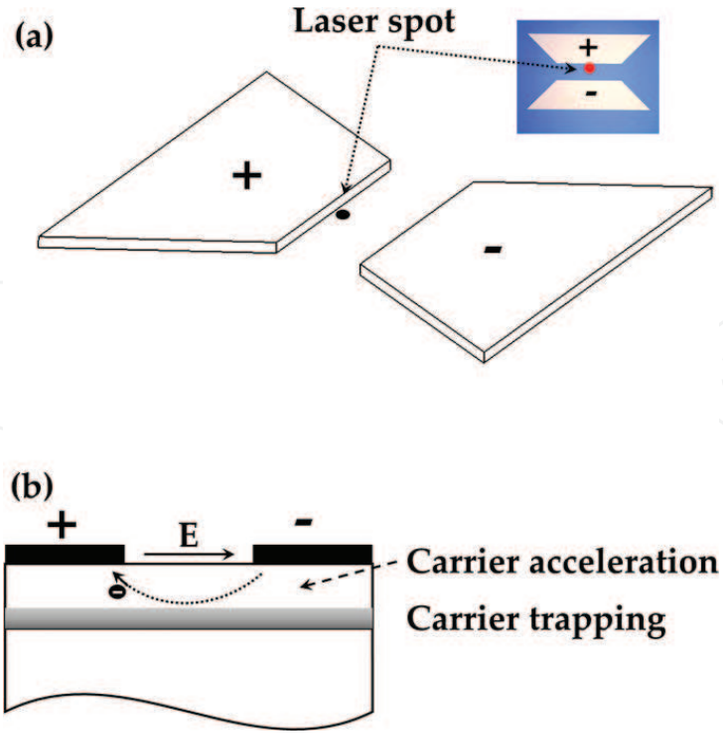

Figure 1. (a) Schematic structure for bow-tie photoconductive antenna (the inset is its photograph). (b) Cross-section of H-implanted GaAs PCAs with acceleration and trapping of photo carriers.

Implantation dose (cm^{-2})	Implantation energy	Ion beam
1×10^{15}	300 KeV	Hydrogen
5×10^{14}	300 KeV	Hydrogen
1×10^{14}	300 KeV	Hydrogen
1×10^{13}	800 KeV	Helium
5×10^{12}	800 KeV	Helium
5×10^{12}	3 MeV	Oxygen
1×10^{12}	3 MeV	Oxygen

Table 1. Process details for all samples with different implantation conditions.

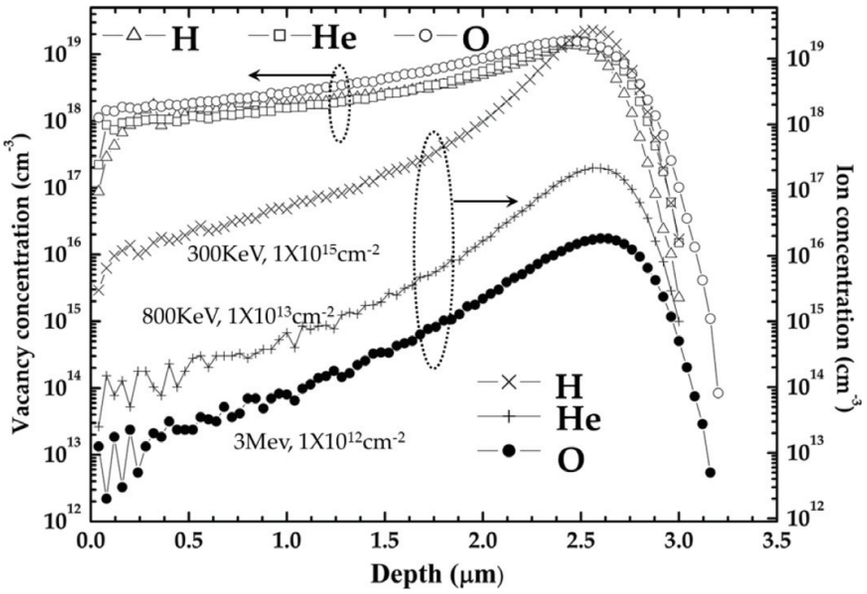

Figure 2. Ion implantation and corresponding vacancy profiles for samples with H dosage of 1×10^{15} cm^{-2}, He dosage of 1×10^{13} cm^{-2}, and O dosage of 1×10^{12} cm^{-2}, calculated by Stopping and Range of Ions in Matter (SRIM), where a Monte-Carlo simulation of 5×10^5 ions was performed for hydrogen, helium, and oxygen. Also, the implantation angle of 7° was used to avoid possible channeling to the crystal axis.

acceleration for THz generations is successfully separated from defects by implantation without obvious decrease of transient mobility in shallow regions. Moreover, the accumulation of photo carriers against the electrical bias was significantly suppressed, avoiding the screen effects by the pump laser (**Figure 1(b)**). Two more sets of samples fabricated on a bare SI-GaAs substrate and 1-μm-thick LT-GaAs grown on an SI-GaAs substrate ("LT-GaAs" hereafter) were prepared for reference.

As shown in **Figure 2**, density profiles of the generated defects and the implanted ions were simulated with the stopping and range of ions in matter (SRIM) program [26]. The implantation conditions for H, He and O are 300 keV, 1×10^{15} cm^{-2}; 800 keV, 1×10^{13} cm^{-2}; and 3 MeV,

1×10^{12} cm^{-2} respectively. At such implantation energies, most ions for all three kinds of samples are implanted far below a surface layer of about 2.5 μm deep where most laser power is absorbed within 1 μm-deep distance and most terahertz power is generated within 2 μm-deep distance. The ion concentration in this region is over three orders of magnitude lower than the peak concentration, whereas the vacancy density profile for all ion beams (H, He, or O) is nearly the same within THz generation distance (∼2 μm below the surface). Another reason to use such implantation energies is to reduce the lifetime and therefore strongly reduce the density of photo carriers produced at a depth of ∼2 μm, which are not only useless for terahertz generation but also cause the saturation for optical pump.

Figure 3 shows the dark currents versus bias voltage (I-V) characteristics for H-implanted and SI-GaAs PCAs without light illumination, measured by a Keysight B1500A semiconductor device analyzer. Currents passing through the SI-GaAs sample quickly exceed the space-charge limited (SCL) electron flows at low voltage of ∼20 V, and then significantly increase by a polynomial V^3 response dominated by a double carrier injection current, as demonstrated in Ref. [21]. It is observed that currents in SI-GaAs antenna under 140 V go up to 10 mA even without any light illumination. This means a considerable temperature increase in active region due to huge heat dissipations, which would affect the efficiency of SI-GaAs antenna and result in electrical breakdown of the device. On the contrary, H-implanted samples follow almost linear dependence of currents on bias voltages in broad range of over 100 V and did not show obvious currents increase of V^3 response even as the bias voltages go up over 200 V. It can be seen that H ions in GaAs extend the linear range of currents dependence on voltages, compared to that for bare SI-GaAs samples. The carrier accumulation near the high electrical field region along anode is significantly suppressed by the corresponding trapping sites and the double carrier injection is eliminated effectively.

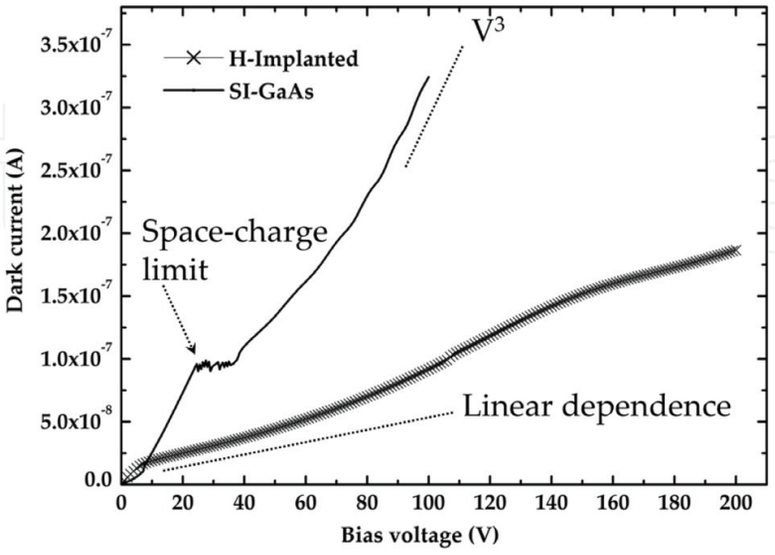

Figure 3. Current-voltage characteristics for SI-GaAs THz antenna and H-implanted one.

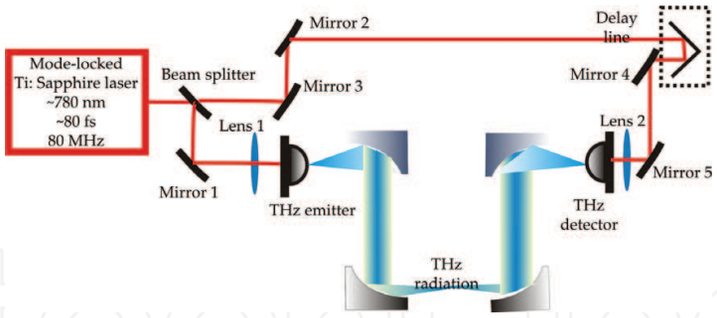

Figure 4. Schematic diagram of THz TDS setup used for measuring electric field of THz pulse.

The setup for characterization of the THz waves is based on a conventional time-domain spectroscopy system (TDS) triggered by a femtosecond laser as shown in **Figure 4**. A mode-locked Ti: Sapphire laser generates 80 fs light pulses at a wavelength of ~780 nm and a repetition rate of 80 MHz. The femtosecond pump pulses were focused by an objective lens with 10 μm-diameter illumination spot on the proximity of anode for a biased photoconductive antenna, which was mounted on the flat side of a Si hemispherical lens with a diameter of 15 mm. The emitted THz radiation was collimated and focused by two pairs of gold-coated off-axis parabolic mirrors onto a photoconductive sampling detector, which was also a photoconductive antenna with bow-tie shape and gap of 20 μm mounted on the back of a Si hemispherical lens with the same diameter. The photoconductive detector was gated by femtosecond probe beam pulses that were separated from the pump beam pulses by a beam splitter.

As_{Ga}^{+}**Figure 5(a)** shows the THz waveforms emitted from GaAs PCAs implanted with H dose of 1×10^{14}, 5×10^{14}, and 1×10^{15} cm^{-2}. The applied bias voltage and pumping power were about 260 V and 60 mW, respectively. The SI-GaAs and LT-GaAs samples were measured under the pump power of 60 mW for reference and the bias voltages for SI-GaAs (40 V) and LT-GaAs (100 V) were kept below breakdown voltages. The waveforms for all samples are normalized at the main peak amplitude in order to see their emission mechanisms clearly. We observe the most sharp THz pulse from GaAs antenna implanted with dose of 5×10^{14} cm^{-2}, and its full width at half maximum (FWHM) of the main peak amplitude is as narrow as 0.3 ps (solid curve), which indicates short carrier lifetimes in the ion-implanted THz emitter and ~0.85 ps lifetime is confirmed by the pump-probe reflectance measurement. The other H-implanted PCAs also demonstrate very short THz pulses with FWHM of 0.31 ps for dose of 1×10^{14} cm^{-2} (dotted curve) and 0.33 ps for dose of 1×10^{15} cm^{-2} (dashed curve). The minimum peak after the main peak for the 5×10^{14} cm^{-2} antenna is sharper than that for all other GaAs PCAs, and its minimum peak before the main peak is also most sharp. The sharp trends of THz signal increase before the maximum THz pulse peak for samples H-1×10^{14} and H-5×10^{14} cm^{-2}, accompanying the current surge in photoconductive region, are completely identical to that case for SI-GaAs sample, which indicates that the carrier mobility in the shallow surface layer for H-1×10^{14} and H-5×10^{14} cm^{-2} PCAs is very close to the mobility of bare SI-GaAs materials. The quite few and uniform point defects (Ga vacancies, As_{Ga}^{+}, etc.) in shallow layer contribute the excellent mobility of these H-implanted samples, compared to LT-GaAs and the sample of H-1×10^{15} cm^{-2}. In order to further identify the uniqueness of these

http://dx.doi.org/10.5772/intechopen.79693

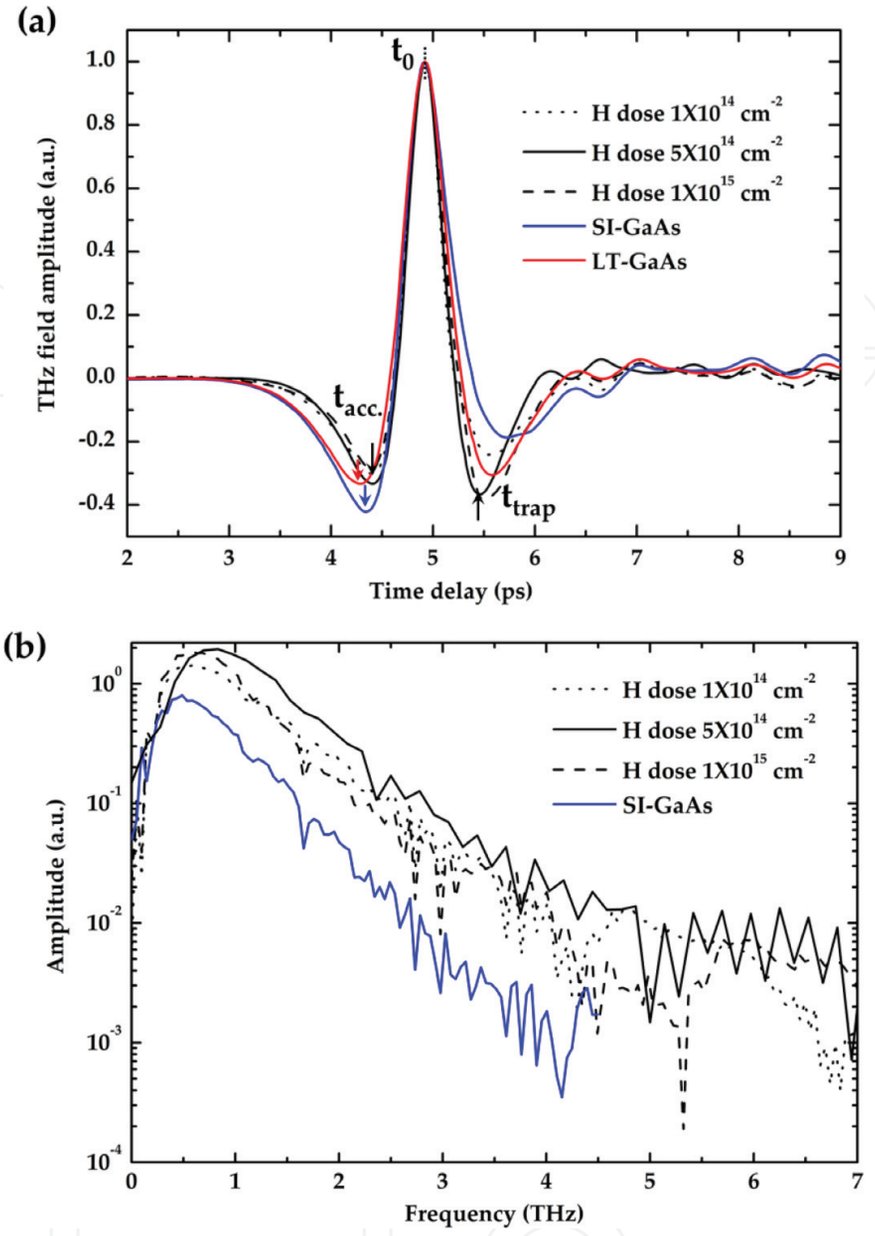

Figure 5. (a) Normalized THz pulses emitted from GaAs antennas of 1×10^{14}, 5×10^{14}, 1×10^{15} cm^{-2}, SI-GaAs, and LT-GaAs. (b) Fast Fourier transformed spectra of THz signals for different GaAs emitters.

ion-implanted GaAs antennas, the fast Fourier transformed (FFT) spectra of the waveform for all implanted PCAs and the reference samples of SI-GaAs are shown in **Figure 5(b)**. We find that ion-implanted GaAs antennas generate THz signals with frequency of over 5 THz and the sample with dose of 5×10^{14} cm^{-2} demonstrates the strongest signals in the high-frequency range of 1 –5 THz. As expected, SI-GaAs samples produce the weakest signals at high frequencies of over 1 THz among all samples.

In order to interpret the THz radiation waveform, we analyze the THz radiation assuming that the emitted field $E_{THz}(t)$ is proportional to the time derivative of the transient current $J(t)$ at far field, as expressed in Eq. (1).

$$E_{THz}(t) \propto \int \frac{\partial J(t)}{\partial t} dxdydz \tag{1}$$

where the integration is taken over the whole device including carrier acceleration layer and carrier trapping layer (**Figure 1(b)**). The transient current depends on the free-carrier concentration n and on the mean velocity v of the electrons:

$$J(t) = -en(t)v(t) \tag{2}$$

the contribution of the holes which have a much smaller mobility is neglected. We analyze the carrier transport based on a set of kinetic equations [27] which can be written as follows:

$$\frac{dn(t)}{dt} = -\frac{n(t)}{\tau_c} + G(t) \tag{3}$$

$$\frac{dv(t)}{dt} = -\frac{v(t)}{\tau_m} + \frac{eE_{loc}}{m^*} - \frac{v(t)G(t)}{n(t)} \tag{4}$$

where G is a photoinjection rate, E_{loc} is the local electric field, τ_c is the free electron lifetime, and τ_m is the momentum relaxation time, which is connected to the mobility of the free electrons in shallow layer.

Based on this theoretical model, the main positive peak observed in the waveforms of **Figure 5 (a)** is attributed to the rises of surge current by photo-carrier injection and the subsequent carrier acceleration under bias fields ($t_{acc.}$ in **Figure 5(a)**), while the second negative peak after the main peak is related to the decay of current governed by the carrier trapping (t_{trap} in **Figure 5(a)**). For the ion-implanted GaAs PCAs, we have to consider the carrier dynamics of acceleration process in shallow layer (<2 μm) and trapping process in the underneath layer (~2.5 μm deep), as shown in **Figure 1(b)**. After laser is absorbed within 1 μm depth, photo carriers are created accordingly and accelerated within 2 μm depth for efficient THz generations. The main peak distribution of implanted ions and related defects at ~2.5 μm depth enables efficient carrier trapping and significantly reduce carrier concentration in the trapping layer (**Figure 1(b)**). If the pump pulse laser width (δt) is larger than the carrier momentum relaxation time (τ_m), and if the carrier lifetime (τ_c) is larger than the pump laser pulse width ($\tau_m < \delta t < \tau_c$), the carrier acceleration and resultant current rise are determined by the pump laser pulse width, which is related to $t_{acc.}$. This is exactly the situation in the shallow laser absorption layer (1 μm deep) for ion-implanted GaAs PCAs; where the momentum relaxation time was estimated to be about 10 fs; the laser pulse width was 80 fs, and the carrier lifetime was over 10 ps (similar to lifetime in bare SI GaAs), respectively. Assuming the transition time for photo carriers from absorption region (1 μm) to the trapping layer (2.5 μm) is shorter than the carrier trapping time, the carrier trapping and corresponding current decay depends on peak concentrations of H ions and implantation-related defects at 2.5 μm depth; considering that carrier transition time is about 100 fs, and the carrier trapping time (t_{trap}) is estimated to be ~0.8 ps for the sample H-5 × 10^{14} cm^{-2}. In the progress of current rise dominated by laser pump, carrier acceleration should not be affected by implantation defects because the ion

concentration in this region is several orders of magnitude lower than the peak concentration and the carrier mobility is able to keep very close to that in SI GaAs. However, the defects for LT-GaAs and the sample of H-1 $\times$ 10^{15} cm^{-2} have decreased the carrier mobility by scattering to some extent that the carrier acceleration turns slow when comparing with SI-GaAs in **Figure 5(a)**, considering the momentum relaxation time (τ_m) may increase to be comparable with the laser pulse width (δt) and the current surge is affected accordingly. Meanwhile, the current decay is dominated by the trapping effect in the underneath THz generation layer. This structure will form vertical confinement for the distribution of photo carriers and block the carriers in SI GaAs substrate, which makes the trapping layer return the original insulating state after the fast carrier trapping. It is noted that the carrier trapping time (t_{trap}) for samples of H-5 $\times$ 10^{14} and H-1 $\times$ 10^{15} cm^{-2} is significantly shorter than that of H-1 $\times$ 10^{14} cm^{-2}, LT-GaAs, and SI-GaAs samples because the latter did not have efficient structures for vertical confinement of photo carriers. Therefore, we conclude that this confinement structure for photoconductive antennas will relieve the screen effect caused by charges accumulation in photoconductive region and reduce the saturation effect by laser excitation.

In **Figure 6(a)**, we show variation of the peak of emitted THz field amplitude with the pump laser power for all samples measured under TDS in **Figure 4**. The bias voltage of 140 V was used. The SI-GaAs sample without H implantation became saturated as the pump laser power exceeded 30 mW, similar to the reports in Refs. [6–10]. Thermal breakdown of SI-GaAs emitters easily occurred as they are saturated by the pump laser and the bias voltage. Normally, SI-GaAs emitters are recommended to operate far enough away from the saturation status. Hydrogen-implanted GaAs emitter with dose of 1 $\times$ 10^{14} cm^{-2} showed relatively linear increase of THz amplitude as the pump laser power. We are able to get the maximum THz field 3.5 times bigger than that from SI-GaAs emitter but no obvious saturation is found at the laser power of over 60 mW. The H-5 $\times$ 10^{14} cm^{-2} sample provides the best performance that almost linear dependence of THz fields emitted on the pump laser power is demonstrated, and the maximum THz field we could obtain from H-5 $\times$ 10^{14} cm^{-2} sample is five times bigger than that from SI-GaAs emitter. It should be emphasized that the H-implanted GaAs with dose of 5 $\times$ 10^{14} cm^{-2} did not show any saturation property with the pump laser approaching 100 mW in the TDS measurement range and the bias voltage increasing up to 260 V. The sample of H-1 $\times$ 10^{15} cm^{-2} showed deteriorated mobility, and THz fields are smaller than those emitted from sample 1 $\times$ 10^{14} cm^{-2}. Because point defects created by H implantation at lower dose of 1 $\times$ 10^{14}–5 $\times$ 10^{14} cm^{-2} are more uniform and fewer, carrier mobility is kept to be very close to that of SI-GaAs with the carrier momentum relaxation time (τ_m) as short as 10 fs also. In the optimum operation conditions (i.e., 80 mW of the laser power and 260 V of the bias voltage for 5 $\times$ 10^{14} cm^{-2} sample versus 30 mW of the laser power and 140 V of the bias voltage for SI-GaAs), THz power emitted from the H-implanted sample was ~100 times bigger than that of traditional SI-GaAs THz emitter.

Figure 6(b) presents the photocurrent as a function of the bias voltage (*I-V*) at a pump laser power of 60 mW for all H-implanted and SI-GaAs samples. Fairly high photocurrents and saturation behavior are observed for the SI-GaAs sample. With increasing the dosage of H implantation, there is continuous decrease in the photocurrents for the ion-implanted GaAs PCAs compared to the conventional SI-GaAs devices, because the presence of a deep trapping layer at 2.5 μm depth blocks the photo carriers in the SI-GaAs substrate. This means that heat

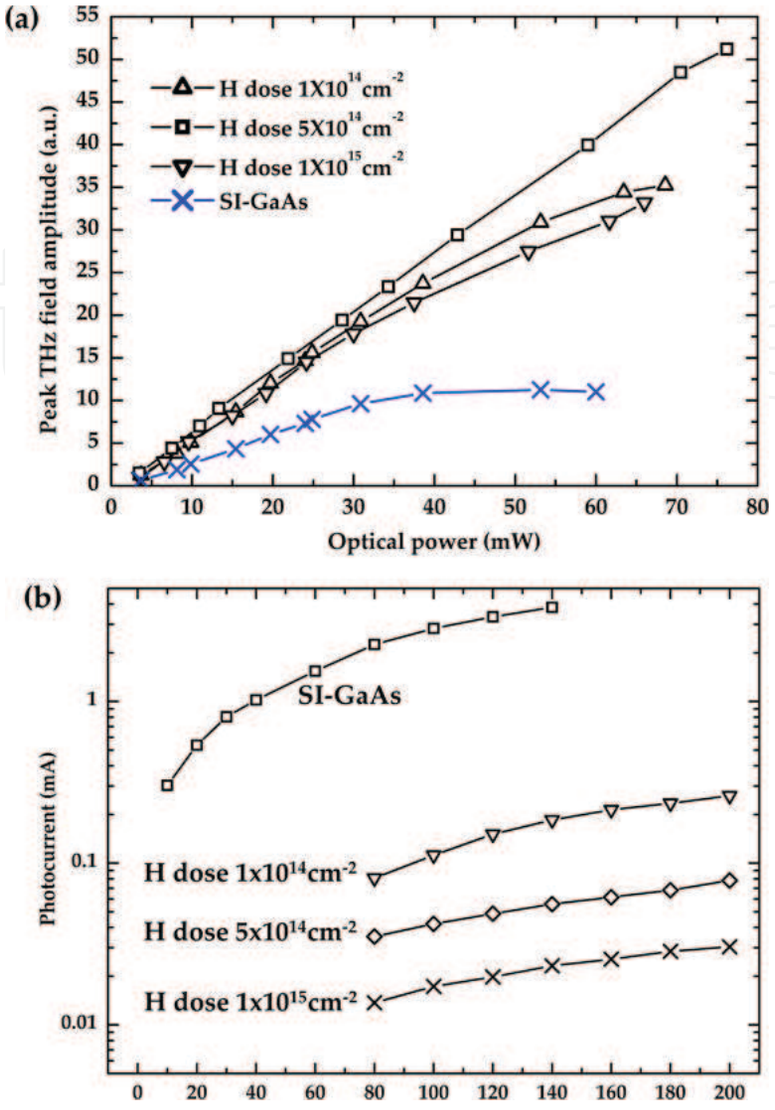

Figure 6. (a) Peak THz field amplitude from GaAs emitters as a function of pump laser power under a bias voltage of 140 V. (b) Photocurrent-voltage (*I-V*) characteristics under excitation at the laser power of 60 mW for H-implanted and SI-GaAs samples. The photocurrent was calculated from the measured current under illumination by subtracting the dark current.

generation will be efficiently suppressed in ion-implanted samples as H dose is increased, then thermal breakdown voltage of GaAs PCAs will become higher as higher dose is utilized. H-implanted GaAs PCAs become electrically robust and are able to stably operate from ~80 to >260 V. To make a rough estimate of improvement in electrical-to-THz power conversion efficiency of the H-implanted GaAs PCAs, we can compare the THz power emission for H-5×10^{14} cm^{-2} sample with conventional SI-GaAs sample without any implantation. As shown in **Figure 6(a)**, the THz field amplitude is about four times more (power will be 16 times) from H-5×10^{14} cm^{-2} sample than SI-GaAs sample under the optical power of 60 mW. Moreover, the corresponding photocurrent for H-5×10^{14} cm^{-2} sample is about 100 times smaller than that for SI-GaAs sample at the same voltage of 140 V. Then, under the same photo-excitation conditions (pump laser power, bias voltage), photocurrent is 100 times smaller, but emitted THz power is 16 times more for H-5×10^{14} cm^{-2} sample than SI-GaAs sample. The electrical to

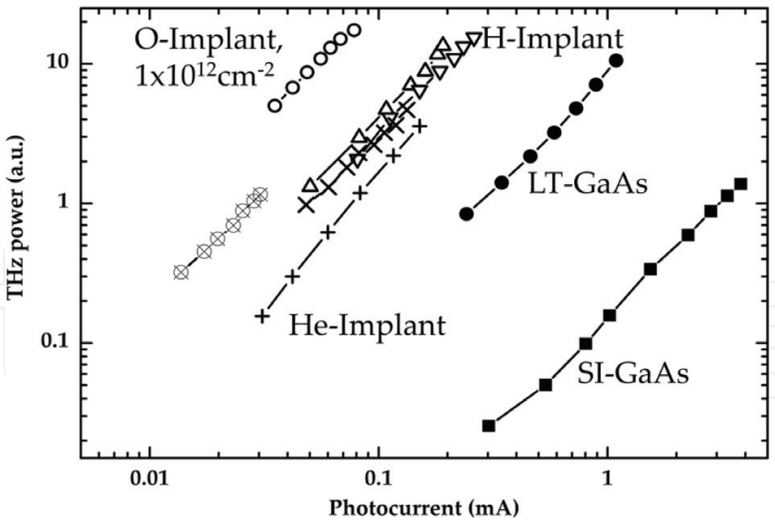

Figure 7. The terahertz power as a function of the photocurrent is represented for ion-implanted GaAs PCAs.

THz power conversion efficiency of H-5 $\times$ 10^{14} cm^{-2} emitter is almost ~1600 times better than SI-GaAs emitter.

To further confirm the mobility in the THz generation layer of ion-implanted PCAs is superior to that of LT-GaAs, **Figure 7** relates the THz radiation power to photocurrents for all ion-implanted PCA samples for a constant laser power in a logarithmic scale. The relationships for all samples are curve-fitted to parallel lines with a slope of 2, indicating the quadratic dependence of the radiation power on the induced photocurrents by the pump laser, and the fact that operation conditions (laser alignment, output THz coupling efficiency, antenna structure, etc.) are the same for all PCAs. The ion-implanted GaAs antennas for H-1 $\times$ 10^{14}, H-1 $\times$ 10^{15}, and O 1 $\times$ 10^{12} cm^{-2} generated stronger THz radiation than LT-GaAs PCAs under the excitation of constant laser power 200 mW, however the DC photocurrents are reduced by about 100 times. This enhancement for THz generation may mainly be attributed to the better quality of photoconductive GaAs with higher mobility than that of LT-GaAs since the conversion efficiency is proportional to the carrier mobility, while the carrier concentration is tightly confined by deep trapping layer at ~2.5 μm-distance in ion-implanted PCAs.

In order to further interpret the THz radiation power and the optical-to-THz conversion efficiency for GaAs PCAs, we deduced the theoretical model accordingly for photoconductive antennas.

According to the Ref. [28], transient photocurrent under fs laser excitations can be written as below Eq. (5).

$$I_{ph} = \frac{eV_b \mu_e \tau \eta_L P_L}{hf_L d^2} \tag{5}$$

where e is the electron charge, f_L is the optical frequency, h is the Planck constant, V_b is the applied bias voltage, μ_e is the electron mobility, τ is the lifetime for photocarriers, η_L is the absorption efficiency for laser illumination, P_L is the incident laser power on the gap, d is the length of photoconductive gap.

Meanwhile, the transient resistance under laser excitations can be approximately formulated as Eq. (6) [15].

$$R_{gap} = \frac{hf_L f_R d^2}{e\mu_e \eta_L P_L} \tag{6}$$

where f_R is the repetition rate for incident fs laser pulses.

Therefore, using Eqs. (5) and (6), we can obtain the expression for the electric power generated between the photoconductive gap, subjected to the pump laser power P_L and the optical-to-THz conversion efficiency for the antenna η_{LE}.

$$P_E = {I_{ph}}^2 R_{gap} = \left(\frac{eV_b \mu_e \tau \eta_L P_L}{hf_L d^2} \right)^2 \frac{hf_L f_R d^2}{e\mu_e \eta_L P_L} = \frac{eV_b^2 \mu_e \tau^2 \eta_L P_L f_R}{hf_L d^2} = \frac{eE_b^2 \mu_e \tau^2 \eta_L P_L f_R}{hf_L} \tag{7}$$

$$\eta_{LE} = \frac{P_E}{P_L} = \frac{eV_b^2 \mu_e \tau^2 \eta_L f_R}{hf_L d^2} = \frac{eE_{loc}^2 \mu_e \tau^2 \eta_L f_R}{hf_L} \tag{8}$$

where E_{loc} is the localized electric field around the anode proximity, for separating the electron-hole pairs, accelerating photocarriers, and the generation of transient photocurrents.

As seen from Eq. (8), the optical-to-THz conversion efficiency is directly proportional to the square of the bias voltage V_b and to the photoconductive material factor $\mu\tau^2$.

According to [28] and the references wherein, the saturation behavior of THz radiation amplitude E_r against the pump intensity F_L or pump power P_L can be expressed as

$$E_r \approx \frac{F_L / F_s}{1 + F_L / F_s} = \frac{P_L / P_s}{1 + P_L / P_s} \tag{9}$$

where F_s, P_s are the characteristic saturation intensity and saturation power for the PC antenna respectively.

$$F_s = \frac{hf_L}{e\mu_e \eta_L} \tag{10}$$

Eq. (10) shows that the saturation behavior for PC antennas will easily take place when the carrier mobility of the photoconductive material is high, and F_s is normally below 100 μJ/cm^2 for conventional SI-GaAs and LT-GaAs PCAs [21–24, 29]. Comparably, our GaAs PCAs based on high-energy ion-implantation did not show any saturation property even when the pump laser intensity increases as high as 10 mJ/cm^2, which indicating the carrier mobility and carrier lifetime are quite low in the deep trapping layer. The carrier mobility and carrier lifetime in the

shallow layer for THz generation are as high as native SI-GaAs materials, which also means that the photoconductive material factor $\mu\tau^2$ is very high to guarantee the high optical-to-THz conversion efficiency for PCAs.

3. Conclusion

In summary, the GaAs PCAs' saturation effect for the excitation of pump laser is efficiently reduced by hydrogen implantation, due to the vertical confinement of photo carriers in H-implanted emitters. THz emitter implanted by H ions of 300 keV and 5×10^{14} cm^{-2} has both excellent mobility and short enough carrier lifetime. Thus, the optical-to-THz conversion efficiency is improved 16 times and the electrical-to-THz conversion efficiency is 1600 times compared to conventional GaAs emitters. Electrically robust H-implanted GaAs PCA is able to operate from ~80 to >260 V without any thermal breakdown. The emitted THz power from H-implanted GaAs antenna is more than two order of magnitude stronger than that from traditional GaAs emitter.

Acknowledgements

This work was supported by the National Natural Science Foundation of China (Grant No. U1613223). The authors acknowledge Ms. Ho Lai Ching, a staff member at the Department of Electronic Engineering, the Chinese University of Hong Kong, Hong Kong, China, for her assistance in equipment maintenance.

Author details

Caiming Sun[1,2]* and Aidong Zhang[1]

*Address all correspondence to: cmsun@cuhk.edu.cn

1 Institute of Robotics and Intelligent Manufacturing (IRIM), The Chinese University of Hong Kong, Shen Zhen, People's Republic of China

2 Department of Electronic Engineering, The Chinese University of Hong Kong, Shatin, NT, Hong Kong, People's Republic of China

References

[1] Dhillon SS et al. The 2017 terahertz science and technology roadmap. Journal of Physics D: Applied Physics. 2017;**50**(4):043001

[2] Lewis RA. A review of terahertz sources. Journal of Physics D: Applied Physics. 2014;**47** (37):374001

[3] Hafez HA, Chai X, Ibrahim A, Mondal S, Ferachou D, Ropagnol X, Ozaki T. Intense terahertz radiation and their applications. Journal of Optics. 2016;**18**(9):093004

[4] Auston DH, Cheung KP, Smith PR. Picosecond photoconducting Hertzian dipoles. Applied Physics Letters. 1984;**45**(3):284

[5] Makram-Ebeid S, Tuck B. Semi-Insulating III-V Materials. Nantwich: Shiva; 1982

[6] Tani M, Matsuura S, Sakai K, Nakashima S. Emission characteristics of photoconductive antennas based on low-temperature-grown GaAs and semi-insulating GaAs. Applied Optics. 1997;**36**:7853

[7] Tani M, Sakai K, Mimura H. Ultrafast Photoconductive Detectors Based on Semi-Insulating GaAs and InP. Japanese Journal of Applied Physics, Part 2. 1997;**36**:L1175

[8] Liu TA, Tani M, Pan CL. THz radiation emission properties of multienergy arsenic-ion-implanted GaAs and semi-insulating GaAs based photoconductive antennas. Journal of Applied Physics. 2003;**93**(5):2996

[9] Salem B, Morris D, Aimez V, Beerens J, Beauvais J, Houde D. Pulsed photoconductive antenna terahertz sources made on ion-implanted GaAs substrates. Journal of Physics. Condensed Matter. 2005;**17**(46):7327

[10] Salem B, Morris D, Salissou Y, Aimez V, Charlebois S, Chicoine M, Schiettekatte F. Terahertz emission properties of arsenic and oxygen ion-implanted GaAs based photoconductive pulsed sources. Journal of Vacuum Science and Technology A. 2006;**24**(3):774

[11] Singh A, Pal S, Surdi H, Prabhu SS, Mathimalar S, Nanal V, Pillay RG, Döhler GH. Carbon irradiated semi insulating GaAs for photoconductive terahertz pulse detection. Optics Express. 2017;**23**(5):6656

[12] Ludwig C, Kuhl J. Studies of the temporal and spectral shape of terahertz pulses generated from photoconducting switches. Applied Physics Letters. 1996;**69**(9):1194

[13] Kono S, Tani M, Sakai K. Ultrabroadband photoconductive detection: Comparison with free-space electro-optic sampling. Applied Physics Letters. 2001;**79**(7):898

[14] Gregory IS, Baker C, Tribe WR, Evans MJ, Beere HE, Linfield EH, Davies AG, Missous M. High resistivity annealed low-temperature GaAs with 100 fs lifetimes. Applied Physics Letters. 2003;**83**(20):4199

[15] Glinskiya IA, Khabibullin RA, Ponomarev DS. Total Efficiency of the Optical-to-Terahertz Conversion in Photoconductive Antennas Based on LT-GaAs and $In_{0.38}Ga_{0.62}As$. Russian MicroElectronics. 2017;**46**(6):408-413

[16] Huang Y, Khiabani N, Shen Y, Li D. Terahertz photoconductive antenna efficiency. In: Proceedings of the International Workshop Antenna Technology (iWAT); Hong Kong, China; 2011. pp. 152-156

[17] Khiabani N, Huang Y, Shen YC, Boyes SJ. Theoretical modeling of a photoconductive antenna in a terahertz pulsed system. IEEE Transactions on Antennas and Propagation. 2013;**61**(4):1538

[18] Taylor AJ, Benicewicz PK, Young SM. Modeling of femtosecond electromagnetic pulses from large-aperture photoconductors. Optics Letters. 1993;**18**(16):1340

[19] Darrow JT, Zhang X-C, Auston DH. Power scaling of large-aperture photoconducting antennas. Applied Physics Letters. 1991;**58**(1):25

[20] Ralph SE, Grischkowsky D. Trap-enhanced electric fields in semi-insulators: The role of electrical and optical carrier injection. Applied Physics Letters. 1991;**59**(16):1972

[21] Yang S-H, Hashemi MR, Berry CW, Jarrahi M. 7.5% Optical-to-Terahertz Conversion Efficiency Offered by Photoconductive Emitters With Three-Dimensional Plasmonic Contact Electrodes. IEEE Transactions on Terahertz Science and Technology. 2014;**4**(5):575

[22] Kim DS, Citrin DS. Coulomb and radiation screening in photoconductive terahertz sources. Applied Physics Letters. 2006;**88**:161117

[23] Rodriguez G, Caceres SR, Taylor AJ. Modeling of terahertz radiation from biased photoconductors: Transient velocity effects. Optics Letters. 1994;**19**(23):1994

[24] Benicewicz PK, Roberts JP, Taylor AJ. Scaling of terahertz radiation from large-aperture biased photoconductors. Journal of the Optical Society of America B: Optical Physics. 1994;**11**(12):2533

[25] Sun CM, Zhang AD. Efficient terahertz generation from lightly ion-beam-treated semi-insulating GaAs photoconductive antennas. Applied Physics Express. 2017;**10**(10):102202

[26] Ziegler JF, Biersack JP, Littmark U. The Stopping and Range of Ions in Solids. Vol. 1. New York: Pergamon; 1985. See also http://www.srim.org/

[27] Jepsen PU, Jacobsen RH, Keiding RH. Generation and detection of terahertz pulses from biased semiconductor antennas. Journal of the Optical Society of America B: Optical Physics. 1996;**13**(11):2424

[28] Smith PR, Auston DH, Nuss MC. Subpicosecond Photoconducting Dipole Antennas. IEEE Journal of Quantum Electronics. 1988;**24**(2):255-260

[29] Chou R-H, Pan C-L. Gap-Dependent Terahertz Pulses from Mid-Size-Gap Multi-Energy Arsenic-Ion-Implanted GaAs Antennas. Japanese Journal of Applied Physics. 2008;**47**(11): 8419-8425

IntechOpen